

Spatial patterns of desynchronization bursts in networks

Juan G. Restrepo*

*Institute for Research in Electronics and Applied Physics and Department of Mathematics,
University of Maryland, College Park, Maryland 20742*

Edward Ott

*Institute for Research in Electronics and Applied Physics,
Department of Physics and Department of Electrical and Computer Engineering,
University of Maryland, College Park, Maryland 20742*

Brian R. Hunt

*Institute for Physical Science and Technology and Department of Mathematics,
University of Maryland, College Park, Maryland 20742*

(Dated: November 21, 2018)

We adapt a previous model and analysis method (the *master stability function*), extensively used for studying the stability of the synchronous state of networks of identical chaotic oscillators, to the case of oscillators that are similar but not exactly identical. We find that bubbling induced desynchronization bursts occur for some parameter values. These bursts have spatial patterns, which can be predicted from the network connectivity matrix and the unstable periodic orbits embedded in the attractor. We test the analysis of bursts by comparison with numerical experiments. In the case that no bursting occurs, we discuss the deviations from the exactly synchronous state caused by the mismatch between oscillators.

PACS numbers: 05.45.-a, 05.45.Xt, 89.75.-k

I. INTRODUCTION

In this paper we study the synchronization of networks of coupled chaotic units that are nearly, but not exactly, identical. In particular, we will be concerned with the spatial patterns of desynchronization bursts that appear when this synchronization is present but intermittent.

When two or more identical dynamical systems are coupled, they can synchronize under appropriate circumstances. The synchronization of chaotic units has been studied extensively [1, 2] and is of significance in biology [3]-[6], laser physics [7]-[9], and other areas [10, 11]. At the same time, the importance of complex networks has been recently appreciated, and progress has been made towards their understanding, including characteristics that might help distinguish qualitatively different networks [12]-[14]. The dynamics of a network of coupled oscillators, and, in particular, its synchronization, has therefore emerged as a subject of great interest.

Pecora and Carroll [15] have proposed a model and analysis method (the *master stability function*) for the study of the stability of the synchronous state of networks of *identical* coupled chaotic units, and this technique has recently been extensively applied [16, 17] to study the synchronization properties of different kinds of networks of identical noiseless chaotic units. These networks include small world [18] and scale-free networks [13].

The analysis of network synchronization by use of the

master stability function technique has so far assumed all the units to be identical and noise-free, so that an exact synchronized state is possible. In practice, however, even if one strives to make the oscillators the same, they are still expected to have a small amount of parameter mismatch, and a small amount of noise is also expected to be present. Under such circumstances, it is known that the synchronization can be interrupted by sporadic periods of desynchronization (bursts). The bursts are typically caused by a periodic orbit that is embedded in the synchronized chaotic attractor and is unstable in a direction transverse to the synchronization manifold. This phenomenon is commonly referred to as *bubbling* [19]-[21], and has been studied extensively for two coupled oscillators [22, 23].

Our purpose in this paper is to study desynchronization bursts in networks of coupled chaotic nonidentical units. (Noise has a similar effect but will not be treated in this paper.) We will use the master stability function approach and, in order to account for the possibility of bubbling, we will also extend this approach to include the stability of embedded periodic orbits. In this case, the bursts have the added feature of having spatial patterns on the network, and we find that these patterns can be predicted from the network connectivity matrix. We will show how these bursts affect different parts of the network in different ways. In particular, we will see how adding connections in a ring can destabilize precisely those nodes that are the most connected, leaving other parts of the network substantially synchronized. (This a somewhat counterintuitive effect related to the fact that, in some cases, increasing the coupling strength destabi-

*Electronic address: juanga@math.umd.edu

lizes the synchronous state [15],[24].)

Arbitrarily small amounts of mismatch will eventually, through the bubbling mechanism, induce desynchronization bursts. We will show that some of the spatial patterns of this possibly microscopic mismatch might get amplified to a macroscopic size in the bursts. We will discuss how one can use knowledge of the parameter mismatch of the dynamical units in the network to decrease the effective size of the mismatch driving the bursts, thereby improving the robustness of the synchronization.

If synchronization is desired, the network and the parameters should be constructed so that the synchronous state for the identical oscillator system is robustly stable (this implies the absence of noise or mismatch induced desynchronization bursts). Even then, the synchronization will not be perfect if the oscillators have parameter mismatch. We will describe the characteristics of the deviations from exact synchronization in terms of the mismatch and the master stability function.

This paper is organized as follows. In Sec. II we review the master stability function approach and apply it to the case of coupled Rössler units. We also discuss the bubbling mechanism by including the embedded periodic orbits in the master stability function analysis. In Sec. III we numerically consider particular networks as examples and show the resulting bursts and their spatial patterns. The patterns we obtain are long and short wavelength modes in a ring and localized bursts produced by strengthening of a single connection in a ring. In Sec. IV we study the effects of the spatial patterns of the mismatch in the development of the bursts. In Sec. V we study the deviations from the synchronous state caused by the mismatch when the synchronous state of the identical oscillator system is stable. In Sec. VI we summarize our conclusions.

II. MASTER STABILITY FUNCTION AND BUBBLING

We now briefly review the master stability function approach introduced in [15]. Consider a system of N dynamical units, each one of which, when isolated, satisfies $\dot{X}_i = F(X_i, \mu_i)$, where $i = 1, 2, \dots, N$, and X_i is the d -dimensional state vector for unit i . In [15] the parameter vectors μ_i are taken to be the same, $\mu_i = \mu$. Here, however, the parameter vectors μ_i are in general different for each unit, but we assume the difference, or *mismatch*, between them to be small. Generalizing the situation treated in Ref. [15] to the case where the individual units are not identical (i.e., the μ_i are not all equal), the system of coupled dynamical units is taken to be of the form

$$\dot{X}_i = F(X_i, \mu_i) - g \sum_{j=1}^N G_{ij} H(X_j), \quad (1)$$

where the coupling function H is independent of i and j , and the matrix G is a Laplacian matrix ($\sum_j G_{ij} = 0$) de-

scribing the topology of network connections. For $i \neq j$, the entry G_{ij} is zero if oscillator i is not connected to oscillator j and nonzero otherwise. The nondiagonal entries of G are determined by the connections, and the diagonal elements are the negative of the sum of the nondiagonal matrix elements in their row. The coupling constant g determines the global strength of the coupling.

Assume first that all the dynamical units are identical, that is, $\mu_i = \mu$. We will refer to this situation as the *idealized* case. In this case there is an exactly synchronized solution $X_1 = X_2 = \dots = X_N = s(t)$ whose time evolution is the same as the uncoupled dynamics of a single unit, $\dot{s} = F(s, \mu)$. This convenient result arises because the Pecora-Carroll model uses the particular choice of coupling in (1) that ensures that the summation is identically zero when all of the X_j are equal. We will denote this synchronization manifold, $X_1 = X_2 = \dots = X_N$, by M . This manifold is a d -dimensional surface within the Nd -dimensional phase space of Eq. (1).

The stability of the synchronized state can be determined from the variational equations obtained by considering an infinitesimal perturbation ϵ_i from the synchronous state, $X_i(t) = s(t) + \epsilon_i(t)$,

$$\dot{\epsilon}_i = DF(s)\epsilon_i - g \sum_{j=1}^N G_{ij} DH(s)\epsilon_j. \quad (2)$$

Let $\epsilon = [\epsilon_1, \epsilon_2, \dots, \epsilon_N]$ be the $d \times N$ matrix representing the deviation of the entire network from the synchronized state. In matrix notation, Eq. (2) becomes

$$\dot{\epsilon} = DF(s)\epsilon - gDH(s)\epsilon G^T. \quad (3)$$

While (3) allows for nonsymmetric coupling, we henceforth assume the coupling matrix G to be symmetric, $G = G^T$. We write the symmetric matrix G as $G = L\Lambda L^T$, where Λ is the diagonal matrix of real eigenvalues $\lambda_1, \lambda_2, \dots, \lambda_N$ of G and L is the orthogonal matrix whose columns are the corresponding real orthonormal eigenvectors of G ($L^T L = I$). Define the $d \times N$ matrix $\eta = [\eta_1, \eta_2, \dots, \eta_N]$ by $\epsilon = \eta L^T$. Then Eq. (3) is equivalent to

$$\dot{\eta} = DF(s)\eta - gDH(s)\eta\Lambda. \quad (4)$$

Componentwise,

$$\dot{\eta}_k = (DF(s) - g\lambda_k DH(s))\eta_k. \quad (5)$$

The quantity η_k is the weight of the k^{th} eigenvector of G in the perturbation ϵ . The linear stability of each ‘spatial’ mode k is determined by the stability of the zero solution of (5). As a consequence of the condition $\sum_j G_{ij} = 0$, there is a special eigenvalue, $\lambda = 0$, whose eigenvector is $\epsilon_N = [1, 1, 1, \dots, 1]$, corresponding to perturbations

in the synchronization manifold M . Since these are not perturbations from the synchronous state, the analysis is focused on the perturbations corresponding to nonzero eigenvalues.

By introducing a scalar variable $\alpha = g\lambda_k$, the set of equations given by (5) can be encapsulated in the single equation,

$$\dot{\eta} = (DF(s) - \alpha DH(s)) \eta. \quad (6)$$

The *master stability function* $\Psi(\alpha)$ [15] is the largest Lyapunov exponent for this equation for a typical trajectory in the attractor. This function depends only on the coupling function H and the chaotic dynamics of an individual uncoupled element, but not on the network connectivity. The network connectivity determines the eigenvalues λ_k (independent of details of the dynamics of the chaotic units). In the sense of typical Lyapunov exponents, the stability of the synchronized state of the network is determined by $\Psi_* = \sup_k \Psi(g\lambda_k)$, where $\Psi_* > 0$ indicates instability. Thus the Pecora-Carroll model cleanly breaks the stability problem into two components, one from the dynamics (obtaining $\Psi(\alpha)$) and one from the network (determining the eigenvalues λ_k).

In contrast to previous work using the master stability function technique, in this paper we are interested in the dynamics of systems in which a small parameter mismatch is present. (Even though in this paper our examples are restricted to the case of mismatch, we emphasize that the same type of bursting phenomenon is expected for identical oscillators if noise is present [19]–[22].) Although the synchronization manifold M present in the dynamics of the idealized system is, in general, not invariant for the system with mismatch, it still may provide a useful approximation to the dynamics in systems with small mismatch. If M is stable for the idealized system, and the mismatch is small enough, then trajectories near M will tend to stay near M , and we regard the vicinity of M to be the “synchronized” state. However, stability of M in the idealized case of identical oscillators is not sufficient to guarantee robust synchronization in a real system where the oscillators are not identical [19]–[22]. While in the vicinity of the synchronization manifold M , a typical trajectory will eventually follow very closely a periodic orbit embedded in the attractor of the idealized system. Some of these periodic orbits may be unstable in a direction transverse to M . When in the vicinity of a transversally unstable periodic orbit, mismatch (or noise) will cause the trajectory have a component in the direction transverse to M and hence to leave the vicinity of the synchronization manifold M . If there are no other attractors, the trajectory will eventually return to the vicinity of M , and the process will repeat, the result being bursts of desynchronization sporadically interrupting long intervals of near synchronization. This type of dynamics is called bubbling [19].

Thus, in the presence of mismatch (or noise), to determine the robustness of synchronization, it is necessary to

determine the transverse stability of the embedded periodic orbits for the noiseless system of identical oscillators. For coupling as in (1), this analysis is independent of the network, and such analyses have been carried out before, e.g., for the analysis of *two* coupled oscillators in Ref. [23]. Equation (6) can be used as before to construct the master stability function for each periodic orbit, if the appropriate periodic trajectories are inserted for $s(t)$ in (3).

As an example, in this paper we work with the Rössler system [25]:

$$\begin{aligned} \dot{x} &= -(y + z), \\ \dot{y} &= x + ay, \\ \dot{z} &= b + z(x - c). \end{aligned} \quad (7)$$

In terms of our previous notation, $d = 3$, $\mu = [a, b, c]^T$, and $X = [x, y, z]^T$. We choose the parameters of the idealized system to be $a = b = 0.2$, $c = 7$. For these parameters, the system has a chaotic attractor (see Fig. 1). We found the periodic orbits embedded in this attractor

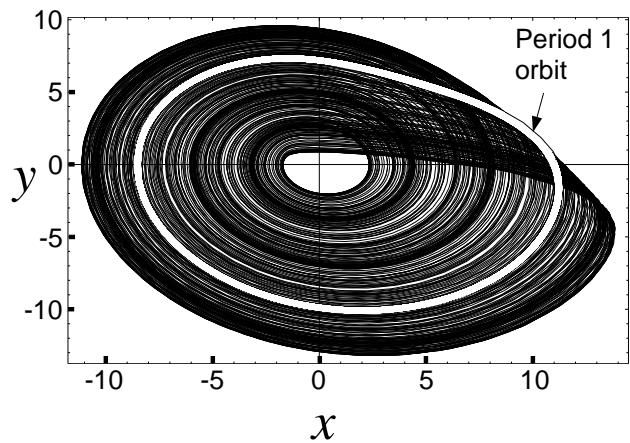


FIG. 1: Rössler attractor (projection onto $x - y$ plane) and embedded period 1 orbit, displayed as a thick white curve inside the attractor. The parameters are $a = b = 0.2$, $c = 7$.

up to period five, and performed the analysis described above on them. We found these orbits by looking at the Poincaré surface of section $\{y = 0, x < 0\}$. To a good approximation, in this surface of section the dynamics is well described by a one dimensional map $x_{n+1} = f(x_n)$, which we approximated using a polynomial fit. From this approximation to f , we determined periodic orbits of period p by using Newton’s method to find the roots of $x = f^p(x)$, where f^p denotes the p times composition of f . We found one period 1 orbit, one period 2 orbit, two period 3 orbits, three period 4 orbits, and four period 5 orbits. Using coupling through the x coordinate,

$$H([x, y, z]^T) = [x, 0, 0]^T, \quad (8)$$

we obtained a stability function $\Psi(\alpha)$ for each orbit, the largest of which will determine if the synchronization is robust. Results are shown in Fig. 2. For all values of α , we found that the master stability function corresponding to the period 1 orbit (thick dashed curve) is larger than that for a typical chaotic orbit (thick continuous curve), as well as those for the other periodic orbits we have found (several of which are shown as thin curves).

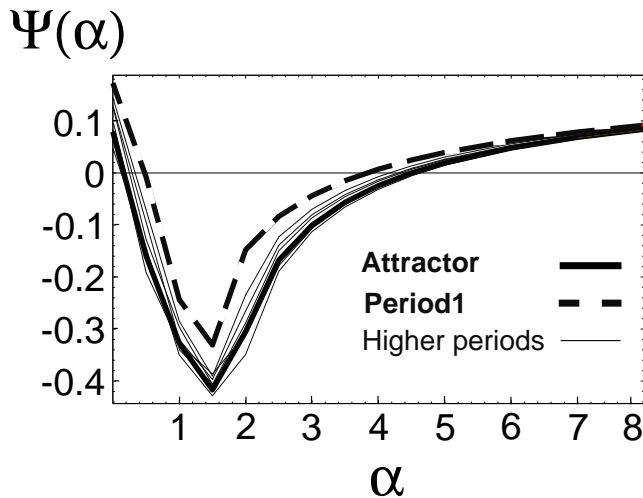


FIG. 2: Master stability function $\Psi(\alpha)$ for a typical trajectory in the attractor (thick continuous curve), for the period 1 orbit (thick dashed curve), and for periodic orbits up to period 4 (thin curves). The curves for the four period 5 orbits are similar to the latter and were left out for clarity.

Based on the discussion above, bubbling induced bursting should occur whenever the master stability function for a typical chaotic orbit in the attractor is negative for $\alpha = g\lambda_k$ and all k , while the period one orbit has positive master stability function for $\alpha = g\lambda_k$ for some value of k . Denoting the master stability function for a typical chaotic orbit by $\Psi_0(\alpha)$ (Thick continuous curve in Fig. 2) and for the period one orbit by $\Psi_1(\alpha)$ (Thick dashed curve in Fig. 2), the *bubbling region* of α corresponds to $\Psi_0(\alpha) < 0$, $\Psi_1(\alpha) > 0$. In our example, this region corresponds to $0.16 < \alpha < 0.48$ or $3.8 < \alpha < 4.5$. The range $0.48 < \alpha < 3.8$ will be referred to as the *stable region*, and the remaining zone will be called the *unstable region*.

If a network of slightly mismatched chaotic systems coupled according to (1) is to be robustly synchronizable without bursts of desynchronization, $g\lambda_k$ must lie in the stable region for all k , where λ_k is the k th eigenvalue of G . If $g\lambda_k$ lies in the stable region for some k and in the bubbling region for other k , then bubbling will typically occur.

III. EXAMPLES

In this Section we provide examples of spatially patterned bursting by considering different configurations of the chaotic units. We will first work with the units connected in a ring with each connection of equal strength. The Laplacian matrix G for this arrangement is

$$G = \begin{pmatrix} 2 & -1 & 0 & 0 & \cdots & 0 & -1 \\ -1 & 2 & -1 & 0 & \cdots & 0 & 0 \\ 0 & -1 & 2 & -1 & \cdots & 0 & 0 \\ \vdots & \vdots & \vdots & \vdots & \vdots & \vdots & \vdots \\ -1 & 0 & \cdots & 0 & 0 & -1 & 2 \end{pmatrix}, \quad (9)$$

and its eigenvalues are given by $\lambda_k = 4 \sin^2(\frac{\pi k}{N})$. Since $\lambda_k = \lambda_{N-k}$, each eigenvalue has multiplicity two, with the exception of $\lambda_N = 0$, and, if N is even, $\lambda_{\frac{N}{2}} = 4$. The matrix G is *shift invariant*, that is, its entries satisfy, modulo N , $G_{i,j} = G_{0,i-j}$. Under these conditions, the diagonalization procedure described above corresponds to a discrete Fourier transform [24]. For the eigenvalue λ_k we choose the eigenvector w_k given by $w_k \propto [\sin(\frac{2\pi jk}{N})]_{j=1}^N$ for $1 \leq k < \frac{N}{2}$, and by $w_k \propto [\cos(\frac{2\pi jk}{N})]_{j=1}^N$ for $\frac{N}{2} \leq k \leq N$. (Due to the degeneracy of the eigenvalues in this case, there is some arbitrariness in choosing the eigenvectors.) Thus, the longest wavelength modes have the smallest eigenvalues, and viceversa.

A. Long wavelength burst

First we consider a case in which bursting of the longest wavelength mode occurs. We consider $N = 12$ and $g = 0.71$. With these values, the longest wavelength mode corresponds to $\alpha = g\lambda_1 \approx 0.19$. This value is in the bubbling region, and all other modes are in the stable region.

To introduce heterogeneity in the dynamical units, we imagine that we have mismatch predominantly in one of the parameters, say a . We simulate this mismatch by adding random perturbations to the parameter a of each oscillator. These perturbations are uniformly distributed within a $\pm 0.5\%$ range; i.e., a_i is chosen randomly in the interval $[0.995a, 1.005a]$, where a is the parameter value of the unperturbed system ($a = 0.2$). The parameters b and c were taken to be the same for each oscillator, $b_i = b = 0.2$, $c_i = c = 7$. How a particular choice of the mismatch affects the bubbling process will be discussed in Section IV.

We solved the 12 coupled differential equations (Eq. (1)) with the initial conditions chosen near the attractor in the synchronization manifold. In Fig. 3 we plot the quantity $x_1 - x_6$ for $1000 \leq t \leq 1600$. Most of the time, this variable is close to zero, as expected if the oscillators are synchronized. Approximately at the time $t = 1380$, this difference grows, reaching magnitudes

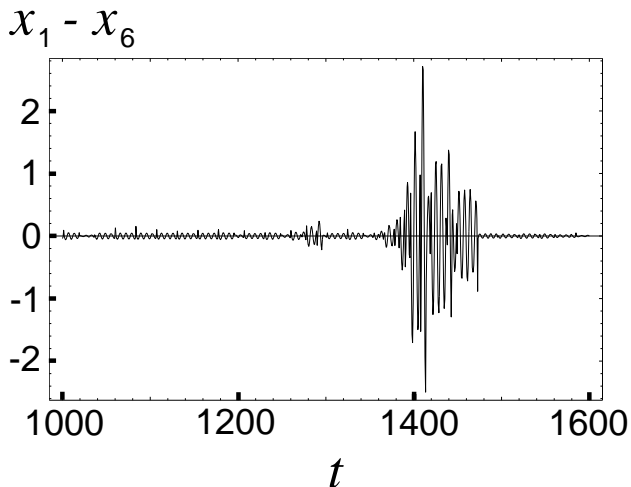


FIG. 3: $x_1 - x_6$ as a function of time for $N = 12$ Rössler systems connected in a ring with $g = 0.71$. Note the desynchronization burst which starts at $t \approx 1380$.

close to 3. By time $t = 1500$, the difference has decreased and is again close to zero.

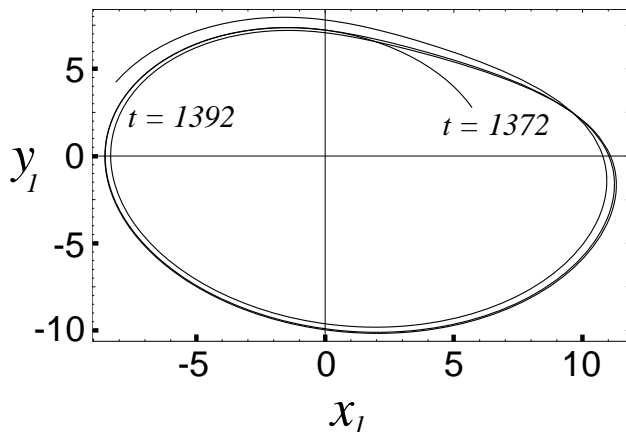


FIG. 4: x_1 versus y_1 for $1372 \leq t \leq 1392$. During this period, which corresponds approximately to the starting point of the burst in Fig. 3, the trajectory follows closely the transversally unstable period 1 orbit embedded in the attractor (See Fig. 1).

To confirm the mediating role of the embedded unstable periodic orbits in the development of the desynchronization burst, we show in Fig. 4 a plot of x_1 versus y_1 from $t = 1372$ to $t = 1392$, which is near the start of the burst. During this time, the trajectory closely follows the period 1 orbit, which is the most transversally unstable of the periodic orbits. Similar observations have been previously reported for *two* coupled chaotic systems [23].

Finally, in Fig. 5 we plot $x_j - x_{j-1}$ as a function of j , the oscillator index, for $t = 1360$ (open triangles), $t = 1385$ (open circles), and $t = 1410$ (open squares).

The desynchronization burst can be observed developing mainly at the longest possible wavelength.

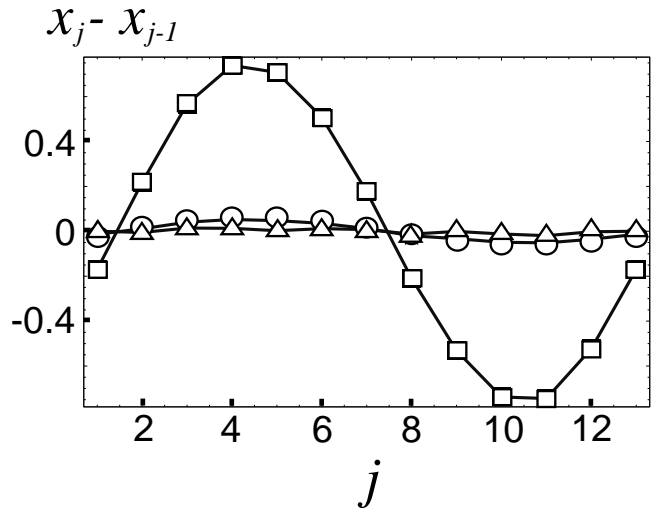


FIG. 5: $x_j - x_{j-1}$ versus the node index j for $t = 1360$ (open triangles), $t = 1385$ (open circles), and $t = 1410$ (open squares). Note that the burst is absent first and grows with a long wavelength pattern.

When subsequent bursts were studied in the same way, it was found that the phase of the long wavelength burst assumed only one value. This is due to the fact that the mismatch is ‘frozen’, that is, each oscillator has a given set of parameters which differs by a given amount from the mean values. This fixed spatial heterogeneity favors certain spatial patterns over others. We will discuss this in more detail in Section IV.

B. Short wavelength burst

Short wavelength bursting can be expected, for example, when $N = 8$ and $g = 1.09$. In this case the value of λ_k corresponding to the shortest wavelength mode yields $g\lambda_k = 4.36$, which is in the bubbling region, while all the other modes are in the stable region. In this case the observation of the bursts is more difficult, as the transversal instability of the orbits and the transversal stability of the attractor are less pronounced (compare $\Psi(4.36)$ for this case vs. $\Psi(0.19)$ for the previous example in Fig. 2). Accordingly, the perturbations of the parameter a were made larger, with perturbations randomly chosen with uniform density within a $\pm 6\%$ range of the ideal values of the parameter ($a = 0.2$). In principle this is not necessary, as a burst will eventually occur after long enough time. In practice, however, it is necessary to reduce the waiting time to a reasonable value. As before, the coupled equations were solved with an initial condition on the synchronization manifold. In Fig. 6 we show $y_2 - y_1$ as a function of time for one choice of initial conditions.

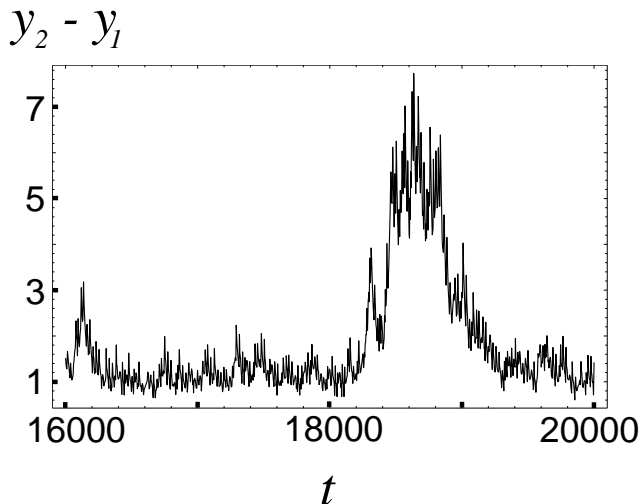


FIG. 6: $y_2 - y_1$ as a function of time for 8 Rössler systems in a ring. The coupling strength g was 1.09. The desynchronization burst develops at $t \approx 18000$, although it is not as sharp due to the smaller magnitude of the transversal Lyapunov exponents ($\Psi(4.36)$ in Fig. 2).

The difference $y_2 - y_1$ is usually positive and of magnitude close to 1. This asymmetry is not a surprise since the oscillators are slightly different. For the relatively large value of the mismatch used, this is the “synchronized state”. It is seen in Fig. 6 that the difference $y_2 - y_1$ increases rapidly at around $t \approx 18400$, and soon reaches values higher than 7. It remains large for a longer time than in the case of the long wavelength burst (see Fig. 3) and decays more slowly as well. This is in qualitative agreement with the smaller absolute values of the master stability functions for the short wavelength mode, both for typical orbits on the attractor and for the periodic orbits.

In Fig. 7 we plot $y_j - y_{j-1}$ as a function of j , the oscillator index, for $t = 17970$, $t = 18270$ and $t = 18570$. As expected, the burst mainly affects the shortest wavelength mode. In order to perform a more quantitative assessment of these observations, we define $\xi_k = \{([\eta_k]_x)^2 + ([\eta_{N-k}]_x)^2\}^{\frac{1}{2}}$ for $1 \leq k < \frac{N}{2}$ and $\xi_{\frac{N}{2}} = |[\eta_{\frac{N}{2}}]_x|$, where $[\eta_k]_x$ is the x component of the three dimensional vector η_k . The quantity η_k is proportional to the magnitude of the vector $[\eta_{1,k} \sin(\frac{2\pi jk}{N}) + \eta_{1,N-k} \cos(\frac{2\pi jk}{N})]$, the component in the Fourier decomposition of the perturbation ϵ associated with modes k and $N - k$. Thus, the quantity ξ_k represents the weight of the modes associated to the eigenvalue λ_k , which have, for $1 \leq k \leq \frac{N}{2}$, a wavelength of $\frac{1}{k}$ th of a full wavelength. In Fig. 8, we plot as a function of time the quantities ξ_k^2 for $k = 1, 2, 3, 4$. The short wavelength mode ($k = 4$, upper curve) is dominant during the burst.

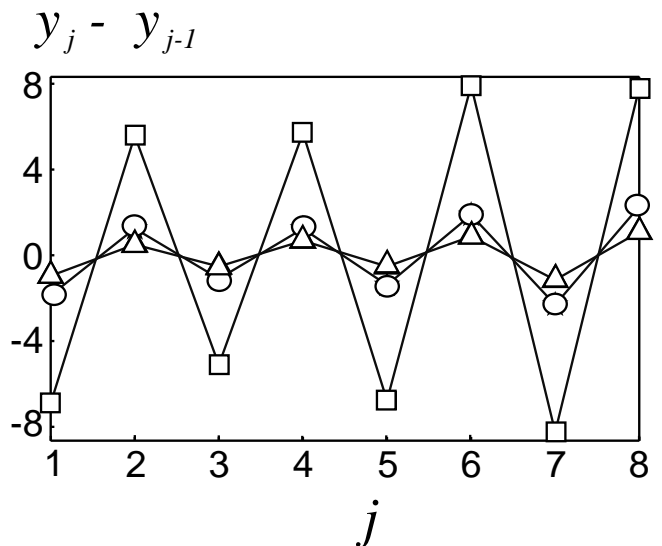


FIG. 7: $y_j - y_{j-1}$ versus the node index j for $t = 17970$ (open triangles), $t = 18270$ (open circles), and $t = 18570$ (open squares). The desynchronization burst has a short wavelength spatial pattern.

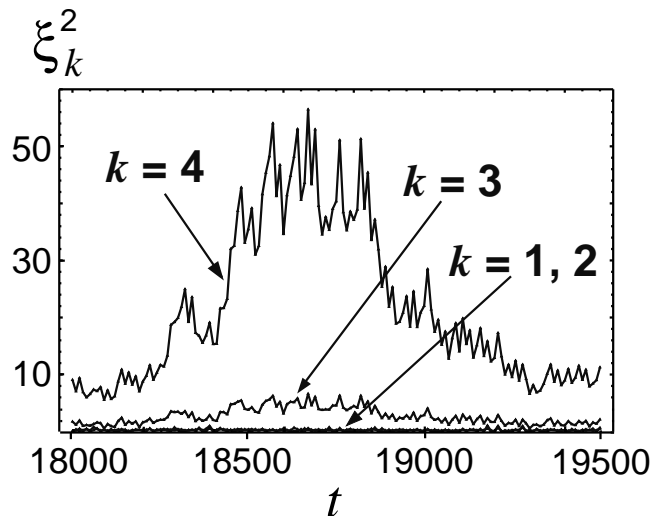


FIG. 8: ξ_k^2 as a function of time for $k = 1, 2, 3, 4$. The shortest wavelength component corresponds to $k = 4$ (top curve). The second shortest one is $k = 3$ (middle curve). The curves corresponding to $k = 1, 2$ are close to zero.

C. Localized burst

In the above examples all links had equal weights. As an example of a case with unequal link weights we consider the case where the previous network is modified by doubling the strength of one of the links. Let the link whose strength is doubled be the link that connects nodes p and $p + 1$. For example, for $p = 4$, $N = 8$, this

yields the Laplacian matrix

$$G = \begin{pmatrix} 2 & -1 & 0 & 0 & 0 & 0 & 0 & -1 \\ -1 & 2 & -1 & 0 & 0 & 0 & 0 & 0 \\ 0 & -1 & 2 & -1 & 0 & 0 & 0 & 0 \\ 0 & 0 & -1 & 3 & -2 & 0 & 0 & 0 \\ 0 & 0 & 0 & -2 & 3 & -1 & 0 & 0 \\ 0 & 0 & 0 & 0 & -1 & 2 & -1 & 0 \\ 0 & 0 & 0 & 0 & 0 & -1 & 2 & -1 \\ -1 & 0 & 0 & 0 & 0 & 0 & -1 & 2 \end{pmatrix}, \quad (10)$$

Adopting the analysis technique of Ref. [26], we can show that such an enhanced connection has the consequence that the largest eigenvalue of G corresponds to an eigenfunction that is exponentially localized to the region near the strong connection. That is, for large N , the components of this eigenfunction decay exponentially as the distance between the localized region and the node corresponding to a component increases. Using the ideas of Ref. [26], we now provide this analysis. The equations for the eigenvector w and eigenvalue λ are

$$\begin{aligned} -2w_{p+1} - w_{p-1} + 3w_p &= \lambda w_p, \\ -w_{p+2} - 2w_p + 3w_{p+1} &= \lambda w_{p+1}, \\ -w_{j-1} - w_{j+1} + 2w_j &= \lambda w_j, \end{aligned} \quad (11)$$

for, respectively, nodes p , $p+1$ and j different from p or $p+1$. Since nodes p and $p+1$ are identical, we can assume, for $k > 0$, $w_{p+1+k} = \pm w_{p-k}$. Furthermore, we propose the ansatz $w_{p+1+k} \propto t^k$, for $k > 0$. This will be a good approximation if the mode is localized (i.e., $|t| < 1$), and the network is big enough that $|t|^{\frac{N}{2}} \ll 1$. In the antisymmetric case, $w_{p+1+k} = -w_{p-k}$, Eqs. (11) yield,

$$\begin{aligned} 5 - t &= \lambda, \\ -t - t^{-1} + 2 &= \lambda \end{aligned} \quad (12)$$

which gives

$$t = -\frac{1}{3}, \quad \lambda = \frac{16}{3}. \quad (13)$$

Compare this eigenvalue with the largest eigenvalue for the network in which all links have equal strength, which has a value of 4. The symmetric solution, $w_{p+1+k} = w_{p-k}$, yields $t = 1$ and $\lambda = 0$, corresponding to the eigenvector $[1, 1, \dots, 1]$ of perturbations in the synchronization manifold. The smallest nonzero eigenvalue remains unchanged.

As an example, we show the localized desynchronization bursts produced by one of these strengthened connections for the case $N = 8$, corresponding to G given by (10) and the illustration in Fig. 9. The parameters of the idealized system are again $a = b = 0.2$, and $c = 7$, with a coupling strength of $g = 0.79$. It is remarkable that despite the small number of nodes, the actual localized eigenvector and eigenvalue agree well with (13) ($\lambda = 5.334\dots$ and $\frac{w_6}{w_5} = -0.334\dots$).

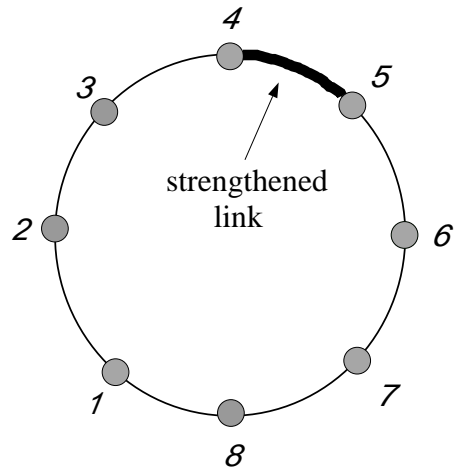


FIG. 9: Arrangement of the dynamical units in a ring with the strength of the connection between nodes 4 and 5 doubled. The matrix G corresponding to this network is in Eq. (10).

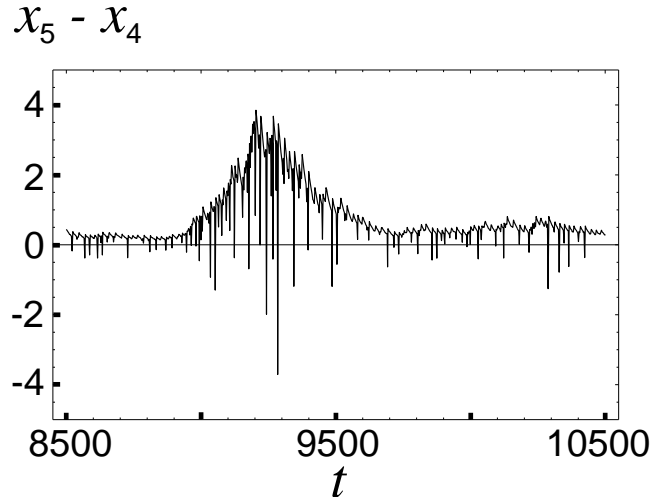


FIG. 10: $x_5 - x_4$ as a function of time for $N = 8$ Rössler oscillators in a ring with the strength of the connection between nodes 4 and 5 doubled. The coupling strength is $g = 0.79$. A desynchronization burst starts approximately at $t \approx 9000$.

In Fig. 10 we show $x_5 - x_4$ as a function of time. As in the short wavelength case, the burst is not very sharp due to the small magnitude of the transversal Lyapunov exponents. Nevertheless, it can be seen that the difference $x_5 - x_4$ increases approximately at $t = 9000$ and returns to a relatively small value after reaching values considerably above the average.

In Fig. 11a we plot the difference between the x coordinate of node j and its mean over all nodes, $x_j - \bar{x}$, where $\bar{x} = \frac{1}{N} \sum_{j=1}^N x_j$, as a function of the oscillator index j , for $t = 8750$ (open triangles), $t = 9000$ (open

circles), and $t = 9250$ (open squares). In Fig. 11b we show the localized eigenvector of the Laplacian G found numerically. As discussed before, the desynchronization

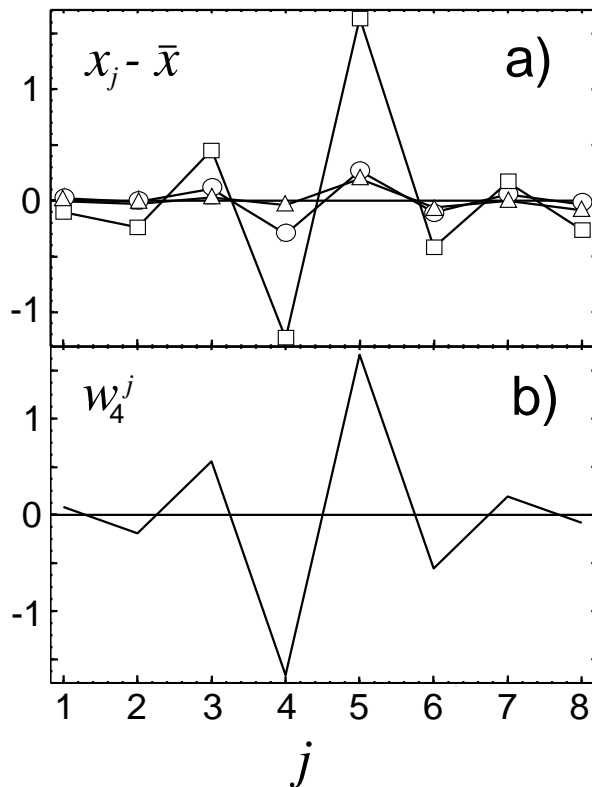


FIG. 11: a) $x_j - \bar{x}$ for $t = 8750$ (open triangles), $t = 9000$ (open circles), and $t = 9250$ (open squares), for the configuration in Fig. 9. The burst develops with the spatial pattern of the localized eigenvector in Fig. 11b. b) Localized eigenvector of matrix G in Eq. (10).

burst affects mainly nodes 4 and 5 (those which share the strengthened connection) and the ones adjacent to them. Nodes 1,2,7 and 8, however, maintain approximate synchronization during the burst.

In Fig. 12 we show the mode weights corresponding to the x coordinate as a function of time. The top curve corresponds to $[\eta_4]_x^2$ (for the localized mode), and the curves close to the horizontal axis to $[\eta_k]_x^2$, $k \neq 4$, for the other modes. (The degeneracy of the eigenvalues is broken by the strengthened connection, so we do not combine $[\eta_k]_x$ and $[\eta_{N-k}]_x$ as before.) Confirming the qualitative similarity between the eigenvector and the spatial pattern of the desynchronization burst observed in Fig. 11, the weight corresponding to the localized eigenvector is seen to be dominant during the period of time in which the burst occurs.

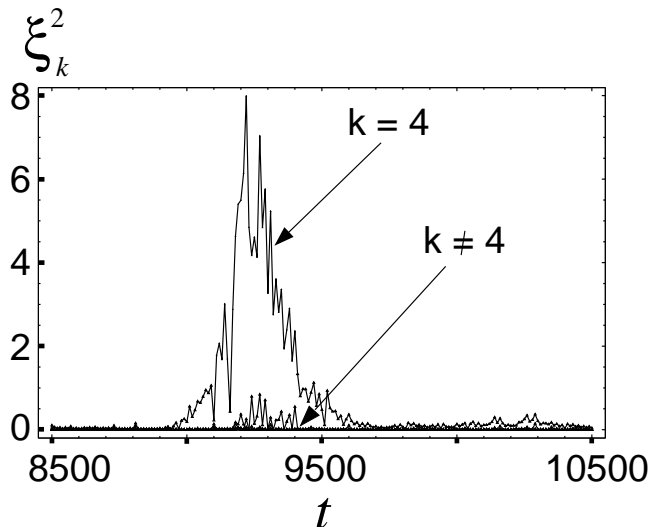


FIG. 12: $[\eta_k]_x^2$ as a function of time for $k = 4$ (top curve) corresponding to the localized mode, and for $k \neq 4$ (bottom curves, close to zero), corresponding to other modes. In the burst, the localized mode is excited first and only after some time are the other modes also somewhat excited. The localized mode is dominant during the burst.

IV. EFFECTS OF THE MISMATCH SPATIAL PATTERNS

In this section we will discuss the effects that the mismatch spatial patterns have on the development of the desynchronization bursts. For these purposes, it will be convenient to rewrite Eq. (1) in the form

$$\dot{X}_i = \bar{F}(X_i) - g \sum_{j=1}^N G_{ij} H(X_j) + Q_i(X_i), \quad (14)$$

where $\bar{F}(X_i) = F(X_i, \bar{\mu})$ with $\bar{\mu} = \frac{1}{N} \sum_{j=1}^N \mu_j$, and $Q_i(X_i) = F(X_i, \mu_i) - \bar{F}(X_i)$. The term Q_i represents the effect of the mismatch and is assumed to be small. As before, we linearize around the synchronous state to get

$$\dot{\epsilon}_i = D\bar{F}(s)\epsilon_i - g \sum_{j=1}^N G_{ij} DH(s)\epsilon_j + Q_i(s), \quad (15)$$

where we have discarded terms of order $Q\epsilon$. With the previous notation and $Q = [Q_1, Q_2, \dots, Q_N]$, we obtain after the diagonalization

$$\dot{\eta}_k = (D\bar{F}(s) - g\lambda_k DH(s))\eta_k + (QL)_k, \quad (16)$$

where $(QL)_k$ is the k 'th column of the $d \times N$ matrix QL . In the ring with equal coupling along each link, the diagonalization procedure corresponds to a Fourier transform. In this case, we see that the mismatch affects the different

modes according to the weight, $(QL)_k$, of this particular mode in its Fourier expansion. In other cases, for example in the localized eigenvector, the strength of the mismatch affecting the localized mode is proportional to the weight of the localized eigenvector in the eigenvector decomposition of the mismatch. We will now discuss two applications of these results.

A. Amplification of mismatch patterns when modes with the same eigenvalue burst

We have shown that the modes of the mismatch force the corresponding modes of the deviations from the synchronous state. When bubbling induced bursting is expected, the size of the mismatch determines the average time between bursts [21]. Thus, the size of the mismatch component in mode k determines the average interburst time when that mode is in the bubbling regime.

When the spectrum of the matrix G is degenerate, the spatial modes of the mismatch play an extra role. All the modes sharing the same eigenvalue λ have the same stability properties, and thus, when the corresponding value $g\lambda$ is in the bubbling zone, all eigenvectors with this eigenvalue are equally likely to appear. The only difference between these modes is the strength with which they are forced, which is determined by the mismatch component in that mode as shown in Eq. (16) (or, if noise is present, by the noise component in that mode).

An example of this situation is the ring with connections of equal strength in the long wavelength bursting scenario. Since the ring is invariant with respect to rotations, the phase of the long wavelength oscillations can not be determined only from the network and dynamics part of the problem. The two modes with the longest wavelength (corresponding to sinusoidal and cosinusoidal oscillations) have the same eigenvalue. It is the mismatch that in this case determines the phase of the long wavelength burst.

We will show how one can determine the phase of the long wavelength desynchronization burst in the case of coupled Rössler systems in a ring with equal coupling along each link. For this system, the mismatch vector $Q_j(X_j)$ is given by

$$Q_j([x_j, y_j, z_j]^T) = \begin{pmatrix} 0 \\ y_j \delta a_j \\ \delta b_j - z_j \delta c_j \end{pmatrix}, \quad (17)$$

where $\delta a_j = a_j - \bar{a}$ and similarly for δb_j and δc_j . We define $\mathcal{F}_k(u) = \sum_{j=1}^N u_j \hat{w}_j^k$, where \hat{w}_j^k is the normalized j 'th component of the k eigenvector described at the beginning of Section III. With this convention, the term $(QL)_k$ in equation (16) is given by

$$(QL)_k = \begin{pmatrix} 0 \\ y \mathcal{F}_k(\delta a) \\ \mathcal{F}_k(\delta b) - z \mathcal{F}_k(\delta c) \end{pmatrix}. \quad (18)$$

Here $\delta a = [\delta a_1, \delta a_2, \dots, \delta a_N]$ and similarly for δb , δc , and y, z are the trajectories around which the linearization was made.

We consider the case in which mismatch in one parameter is dominant, for example a . The mismatch in the parameters b and c will be assumed negligible compared with that in a , so that $\delta b, \delta c \ll \delta a$. In this case, only the second component of (18) is of relevance. Thus modes η_1 and η_{N-1} are excited with a strength proportional, respectively, to $\mathcal{F}_1(\delta a)$ and $\mathcal{F}_{N-1}(\delta a)$; see (16). The magnitude of η_k will be proportional to $\mathcal{F}_k(\delta a)$, and thus the excitation of the long wavelength mode (which is the only one for which perturbations grow) is proportional to

$$\mathcal{F}_1(\delta a) \sin\left(\frac{2\pi j}{N}\right) + \mathcal{F}_{N-1}(\delta a) \cos\left(\frac{2\pi j}{N}\right) \quad (19)$$

$$\propto \sin\left(\frac{2\pi j}{N} + \phi\right), \quad (20)$$

where $\tan \phi = \mathcal{F}_{N-1}(\delta a)/\mathcal{F}_1(\delta a)$.

We now show results of numerical simulations illustrating the above. The parameters N and g will be as in the long wavelength example in the previous section. We use the same random set of perturbations used in that example. As described above, we obtained the phase ϕ of the long wavelength component of the vector δa_i . In Fig. 13 we plot $y_j - y_{j-1}$ for different times during a burst (filled symbols). In the same Figure, we plot a scaled version of $\sin\left(\frac{2\pi j}{12} + \phi\right) - \sin\left(\frac{2\pi(j-1)}{12} + \phi\right)$ (open circles). The phase of the desynchronization burst is in agreement with that of the long wavelength component of the mismatch.

When the mismatch affects predominantly one parameter as in this case, the phase of the bursts can be predicted as described above. When mismatch in different parameters is comparable, the phases of the long wavelength modes of the different parameter mismatches compete and the bursts develop with one of these phases or with a combination of them.

It must be emphasized that this analysis is possible only when there is a degeneracy of the eigenvalues. For example, the location of the localized burst can not be determined in this way, as it is fixed in the position of the strengthened link. In this case, the mismatch component in the localized mode would only affect the average time between bursts.

B. Artificial suppression of unstable modes using knowledge of the mismatch

We will now discuss another consequence of Eq. (16). We imagine a situation where we are given a number of nearly identical oscillators that we are to connect in a network which we desire to be in synchronism as much as possible. Furthermore, we imagine that, through measurements made individually on each oscillator, we are

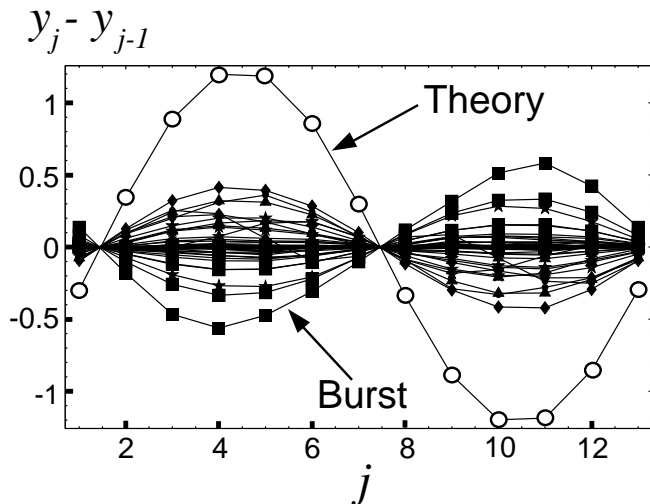


FIG. 13: $y_j - y_{j-1}$ for different times during a burst (filled symbols), and a scaled version of $\sin\left(\frac{2\pi j}{12} + \phi\right) - \sin\left(\frac{2\pi(j-1)}{12} + \phi\right)$ with ϕ as given in the text (open circles). The phase of the burst spatial pattern coincides with the phase of the long wavelength component of the mismatch.

aware of the amount of mismatch in each oscillator. The question we address is this: Using our knowledge of the individual mismatches, how should we arrange the oscillators in the network so as to best suppress the frequency of desynchronization bursts? To answer this question, we note that, according to the previous discussion, we should reduce the mismatch component in the mode which is in the bubbling region. Since the size of the mismatch affects the average interburst time [21], reducing this component is desirable if one wants to improve the quality of the synchronization. This can be accomplished by judiciously arranging the dynamical units so that the k 'th mode of the mismatch is minimized when the corresponding value $g\lambda_k$ is in the bubbling region. For example, to suppress long wavelength bursts, one may arrange the units so that the parameter errors alternate above and below the mean. To suppress the localized bursting described in the previous section, one could arrange the units so that those with the more similar parameters are the ones in the region of the strengthened connection.

As a concrete example, we test this idea using simulations for the case of short wavelength bursting presented in the previous Section. We again assume for simplicity that mismatch in the parameter a is dominant. We generate random perturbations in the parameter a within a $\pm 6\%$ range of the value $a = 0.2$, as explained in the previous section. With this set of parameters given, we set up the dynamical units in the ring using two different permutations of their positions. One of them (a_s) has a smaller and the other (a_l) a larger short wavelength component $\mathcal{F}_4(a)$ than the original random sequence. The ratio $\mathcal{F}_4(a_l)/\mathcal{F}_4(a_s)$ is approximately 15. In Fig 14 we

plot $x_1 - x_2$ as a function of time for configuration a_{large} (top curve) and for configuration a_{small} (bottom curve). The difference $x_1 - x_2$ is much smaller in the former case

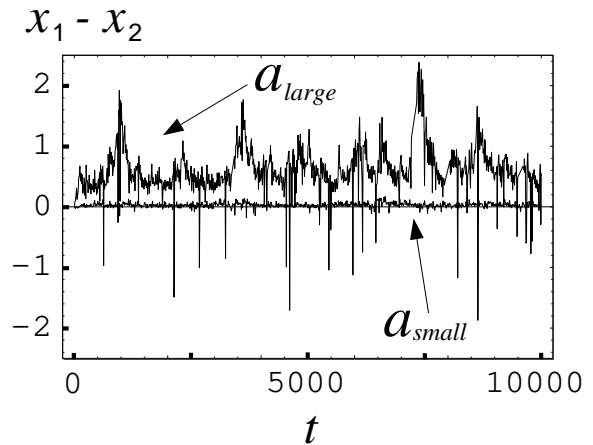


FIG. 14: $x_1 - x_2$ as a function of time for a configuration of oscillators with a large (top curve) and with a small (curve closer to zero) short wavelength component of the mismatch. The quality of the synchronization is much better in the second case.

than in the latter, roughly by a factor of 15, as can be expected from the ratio $\mathcal{F}_4(a_{large})/\mathcal{F}_4(a_{small})$. This qualitative example illustrates how one can use knowledge of the mismatch to suppress undesired instabilities.

V. SPATIAL PATTERNS OF DEVIATIONS FROM THE STABLE SYNCHRONOUS STATE

So far, we have concentrated in the case in which the value of $g\lambda_k$ is in the bubbling regime for one mode k and in the stable regime for the other modes, so that desynchronization bursts occur sporadically. As we have seen, these bursts present spatial patterns on the network.

If synchronization is desired, one would might try to avoid the bubbling regime by designing the network and adjusting the coupling strength so that all the modes lie in the stable zone. One would also strive to reduce the mismatch, but as mentioned before, there are practical limitations on how much one can make the oscillators exactly the same.

If $\Psi(g\lambda_k)$ is negative for all modes (indicating transversal stability of the synchronous state) one can have, depending on the degree of transversal stability, fair synchronization even with relatively large amounts of mismatch. If one is to operate under such conditions, it is important to know the characteristics of the deviations from the synchronous state.

Thus we ask in this scenario: How large are the spatial patterns of the deviations from the synchronous state, and how does this depend on the mismatch and on the degree of transversal stability?

The spatial modes of these deviations obey Eq. (16). In the absence of the term $(QL)_k$, the zero solution is stable, and typical perturbations from it decay, having a negative Lyapunov exponent given by $h_k \equiv \Psi(g\lambda_k)$. The first term in the right hand side of Eq. (16) can be thought of as a damping term with a damping rate given by h_k , and the second term, $(QL)_k$, as a forcing term. Since we are considering the stable case, these two factors, on average, cancel each other. By definition, the Lyapunov exponent for the system without mismatch is given by $h_k = \langle \frac{\eta_k^T (D\bar{F} - g\lambda_k DH) \eta_k}{|\eta_k|^2} \rangle$, where the angle brackets indicate time average. Assuming a solution η_k of the system with mismatch to yield the same value of this time average, we left multiply Eq. (16) by $\eta_k^T |\eta_k|^{-2}$ and average to obtain

$$|h_k| \approx \langle \frac{\eta_k^T (QL)_k}{|\eta_k|^2} \rangle \sim \langle \frac{|(QL)_k|}{|\eta_k|} \rangle, \quad (21)$$

where the angle brackets indicate time average. This leads to the following rough estimate,

$$\langle |\eta_k| \rangle \sim \frac{\langle |(QL)_k| \rangle}{|h_k|} \quad (22)$$

As an example we consider Rössler units in a ring with all connections of equal strength. We choose $N = 8$, $g = 0.6$ ($\Psi(g\lambda_k) < 0$ for all values of k). Furthermore, we add a random perturbation to the parameter a of each oscillator chosen uniformly from within a $\pm 0.1\%$ range of $a = 0.2$.

In Fig. 15 we show, for $k = 1, \dots, 7$, the quantities $\langle |\eta_k| \rangle$ (squares), $\langle |(QL)_k| \rangle$ (triangles), and $\frac{\langle |(QL)_k| \rangle}{|h_k|}$ (stars). The magnitudes of the forcing term for the differ-

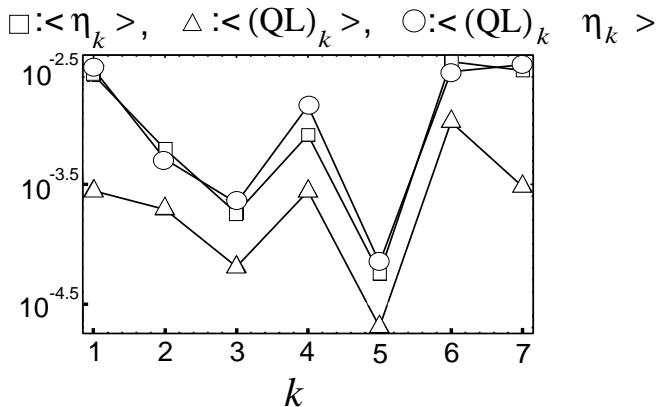


FIG. 15: $\langle |\eta_k| \rangle$ (open squares), $\langle |(QL)_k| \rangle$ (open triangles), and $\frac{\langle |(QL)_k| \rangle}{|h_k|}$ (open circles) for $N = 8$, $g = 0.6$, $k = 1, \dots, 7$. The forcing term (open triangles) roughly determines the response (open squares). The corrected forcing term (open circles) matches well the response (open squares).

ent modes ($\langle |(QL)_k| \rangle$) span roughly two orders of magnitude, and the magnitude of the response ($\langle |\eta_k| \rangle$) looks roughly proportional to the latter. When the forcing term is corrected by dividing it by the magnitude of the corresponding Lyapunov vector $|h_k|$, the resulting quantity ($\frac{\langle |(QL)_k| \rangle}{|h_k|}$) matches very well the observed response.

VI. CONCLUSIONS

We have studied the stability properties of the synchronized state in a network of coupled chaotic dynamical units when these have a small heterogeneity. We have shown that when the dynamical units that are coupled in a network are slightly different, the synchronized state can be interrupted by large infrequent desynchronization bursts for some values of the parameters. The range of the parameters for which this phenomenon is expected can be obtained by performing a master stability function analysis of the chaotic attractor and of the periodic orbits embedded in it.

The desynchronization bursts are induced by the bubbling phenomenon, and have spatial patterns on the network. These spatial patterns can be predicted from the eigenvectors of the Laplacian matrix G and the master stability functions mentioned above. We showed examples illustrating the development of bursts with spatial patterns. One of our examples showed that the strengthening of a single connection might destabilize the nodes near this connection, while leaving the rest of the network approximately synchronized.

Direct measurement of the parameter mismatch in the elements of a network might prove useful. We discussed how this knowledge could be used to reduce the frequency of bursts and to predict the relative weights of different spatial patterns in a burst. We also discussed how one could, from knowledge of the mismatch and of the master stability function, describe the spatial patterns and magnitude of the deviations from the synchronized state when the synchronization of the corresponding identical unit system is robust.

We emphasize that although we did not discuss the effects of noise, the phenomenon described in this paper also occurs for noisy identical oscillators. Desynchronization bursts with spatial patterns are expected for noisy, identical oscillators if one has them for noiseless, non-identical oscillators. The difference is that the parameter mismatch is always ‘frozen’, in the sense that the mismatch is always the same for each oscillator, whereas for noise this is not the case.

Acknowledgements: This work was sponsored by ONR (Physics) and by NSF (contracts PHYS 0098632 and DMS 0104087).

-
- [1] L.M. Pecora, T.L. Carroll, G.A. Johnson, D.J. Mar, and J.F. Heagy, *Chaos* **7**, 520 (1997).
- [2] A. Pikovsky, M. Rosenblum, and J. Kurths, *Synchronization: A universal concept in nonlinear sciences*, (Cambridge University Press, Cambridge, 2001).
- [3] R.C. Elson, A.I. Selverston, R. Huerta, N.F. Rulkov, M.I. Rabinovich, and H.D.I. Abarbanel, *Phys. Rev. Lett.* **81**, 5692 (1998).
- [4] J. Jalife, *J. Physiol.* **356**, 221 (1984).
- [5] R.E. Mirollo and S.H. Strogatz, *SIAM J. Appl. Math.* **50**, 1645 (1990).
- [6] E. Mosekilde, Y. Maistrenko, and D. Postnov, *Chaotic Synchronization: Applications to Living Systems* (World Scientific, Singapore, 2002).
- [7] R. Roy and K.S. Thornburg, *Phys. Rev. Lett.* **72**, 2009 (1994).
- [8] J. García-Ojalvo, J. Casademont, C.R. Mirasso, M.C. Torrent, and J.M. Sancho, *Int. J. Bifur. Chaos* **9**, 2225 (1999).
- [9] A. Uchida, S. Kinugawa, T. Matsuura, and S. Yoshimori, *Phys. Rev. E* **67**, 026220 (2003).
- [10] W. Wang, I.Z. Kiss, and J.L. Hudson, *Chaos* **10**, 248 (2000).
- [11] K.M. Cuomo and A.V. Oppenheim, *Phys. Rev. Lett.* **71**, 65 (1993).
- [12] M.E.J. Newman, *SIAM Review* **45**, 167 (2003).
- [13] A.-L. Barabási, and R. Albert, *Science* **286**, 509 (1999).
- [14] M. E. J. Newman and J. Park, *Phys. Rev. E.* **68**, 036122 (2003).
- [15] L.M. Pecora and T.L. Carroll, *Phys. Rev. Lett.* **80**, 2109 (1998).
- [16] M. Barahona and L.M. Pecora, *Phys. Rev. Lett.* **89**, 054101 (2002).
- [17] T. Nishikawa, A. E. Motter, Y.-C. Lai, and F. C. Hoppensteadt, *Phys. Rev. Lett.* **91**, 014101 (2003).
- [18] D.J. Watts and S.H. Strogatz, *Nature*, **393**, 440 (1998).
- [19] P. Ashwin, J. Buescu, and I. Stewart, *Phys. Lett. A* **193**, 126 (1994).
- [20] S.C. Venkataramani, B.R. Hunt, and E. Ott, *Phys. Rev. E* **54**, 1346 (2003).
- [21] A.V. Zimin, B.R. Hunt, and E. Ott, *Phys. Rev. E* **67**, 016204 (2003).
- [22] N.F. Rulkov and M.M. Sushchik, *Int. J. Bifur. Chaos* **7**, 625 (1997).
- [23] J.F. Heagy, T.L. Carroll, and L.M. Pecora, *Phys. Rev. E* **52**, R1253 (1995).
- [24] J.F. Heagy, L.M. Pecora, and T.L. Carroll, *Phys. Rev. Lett* **74**, 4185 (1995).
- [25] O.E. Rössler, *Phys. Lett. A* **57**, 397 (1976).
- [26] X. Liu, G. Strang, and S. Ott, *Siam J. Discrete Math.* **16**, 479 (2003).